BLOOD FLOW INSPECTION IN FUSIFORM ABDOMINAL AORTIC ANEURYSMS

ALI J. ALI¹, MIQDAM T. CHAICHAN²,* HASAN S. MAJDI³, KADHUM A. JEHHEF⁴

¹Department of Biomedical Engineering, University of Technology, Baghdad 10066, Iraq
 ²Energy and Renewable Energies Technology Centre,
 University of Technology, 35050 Baghdad-Iraq
 ³Department of Chemical Engineering and Petroleum Industries,
 Al-Mustaqbal University College, 51001 Hillah, Babylon, Iraq,
 ⁴Engineering Technical College-Baghdad, Middle Technical University, Baghdad, Iraq
 Corresponding Author: miqdam.t.chaichan@uotechnology.edu.iq

Abstract

An experimental and numerical examination was presented to study the effect of various dimensions and configurations for the fusiform abdominal aortic aneurysms FAAA. The experimental work includes a test section made from acrylic plastic with inlet and exit sections of 10 cm. The test section represents the FAAA region, and it has a semi-major axis that represents the longest radius of FAAA and a semi-minor axis that represents the shortest radius of FAAA. The results indicated that the friction factor increased with increasing the semi-major axis of FAAA, and the maximum friction factor is obtained when test model-6 of a = 36 mm and b = 7 mm by 62% as compared with without an aneurysm model. The highest wall shear stress levels are obtained downstream of the FAAA for model-4, with a = 72 mm and b = 14 mm by about 77%. The numerical results showed that the highest values of friction factor and wall shear stress levels were obtained in the upstream and downstream of FAAA. Also, the friction coefficients upstream and downstream are 0.282 and 0.235, respectively, and the wall shear stresses obtained upstream and downstream are 0.473 and 0.243, respectively, for model 4.

Keywords: Aortic Aneurysms, Fusiform, Hemodynamic, Newtonian Blood flow, Vascular disease.

1. Introduction

An abdominal aortic aneurysm (FAAA) is a vascular disease that happens due to the weakness of the aorta and develops in its wall a balloon-like structure. Aneurysm is an increase of more than twice the proximal artery size. Aneurysm in arteries is divided hooked on three main forms: in the form of a spindle, where the expansion is symmetrical; sacred, when the expansion is on one side of the artery; and in the form of a spindle, in which all sides are enlarged, but asymmetrical. The diameter of the aneurysms can be four times the normal diameter of the aorta and can rapidly increase 0.2-1.0 cm/year until sudden rupture occurs and the men suffer more than women in a 4:1 ratio [1].

Several revisions that carried out to the presentation of blood flow hemodynamic in the FAAA by utilising stable and pulsating flow conditions. The Particle Image Velocimetry PIV technique is used for Reynolds numbers of 400 to 1400 and Womersley numbers of 17 to 22 for stable and pulsating conditions [2]. The results showed that under stable conditions, the circulating vortex occupied the entire circular convex of the AAA.

In addition, the theoretical study uses 3D computer models, and FEM analysis (a non-linear hyperplastic typically that depicts the aneurysm wall behaviour) was used [3]. They found that FAAA wall tension is the best indication of high voltage regions of the FAAA diameter on behalf of high-risk patients with rupture and who subsequently need a speedy recovery.

Seven different FAAA models were investigated by Peattie et al. [4]. It showed that WSS seemed steady at the top of the tube, and then it decreased in bloating, and then the WSS increased again at the distal bulge end. However, a study of the vortex-like vortices (FAAA) is dependent upon the flow wave shape, and the effects of vortices can growth the walls static pressure of FAAA, and this leads to an increase in the wall shear stress that was reported by Deplano et al. [5].

Some aortic models were simulated numerically using pulse-entry waves for both rest and training conditions. A (LES) procedure to study various models of Newtonian and non-Newtonian with pulsating blood hemodynamic conditions over a restricted state due to aneurysm in the arteries was implemented by Molla [6]. They found that there is a large area of recirculation within the aneurysm there.

Also, Altuwaijiri [7] found that the FAAA repair requires surgery, but the operation has an about 5% mortality rate in patients with stable FAAA. In addition, a decision is made to perform the procedure for an aortic diameter of 5 cm as a maximum. A new EVAR method in the silico methodology is used to calculate the final state of the stent graft after interference was introduced [8].

Moreover, Jayendiran et al. [9] suggested combining the high mathematical (CFD) and 4D MRI stream to investigate the advanced variations in arterial wall rupture index (RPI) and blood flow caused by morphological changes in the aorta. They studied the number of indicators such as (WSS), average WSS (TAWSS), viscosity, and relative residence time (RRT).

However, Bauer et al. [10] studied the effects of blood flow on acute shear stress (WSS) under general aneurysm in the abdomen under a realistic pulsed flow using the Doppler Laser Speedometer (LDV), magnetic resonance velocity (MRV), and (CFD). Boltzmann method (LBM) was used by Afrouzi et al. [11] for

developmental sculptures of the arterial blood flow model. They performed simulations of two types of aneurysms in the first case, and they used three electrical ancestors, 0.6, 0.8, and 1.0, with Reynolds number 100, and in the second case, they used three Reynolds numbers 100, 150, and 200, and three Womersley.

Moreover, Dubey et al. [12] presented a 2D numerical study of the hemodynamic of the blood over a sick permeable aneurysm in the artery. They studied the effect of several parameters, such as thermoplastic, Grashof No., Brownian motion, a ratio of parameters Sisko, and thermoplastic buoyancy coefficient on speed, temperature, and pressure of blood.

Wang et al. [13] attempted to solve the problem of the interaction of fluid structure with blood flow in arteries by consuming the FEM with submerged boundaries and mesh. Also, Djorovic et al. [14] studied the effect of the presence of abdominal aortic aneurysm on the blood flow in the aortic scheme and leaving the iliac joint aneurysm before placing the graft stent. Reorowicz et al. [15] investigated and visualised the hemodynamic of blood before and after stent implantation using numerical simulation in a patient-specific model of the abdominal aortal aneurysm, and Panchal et al. [16] performed a numerical analysis of the AAA-related hemodynamic.

Using Open-FOAM, axisymmetric simulations of pulsatile non-Newtonian blood flow are carried out to better understand the blood flow phenomena in a double-fusiform aneurysm. Hussain et al. [17] looked at the flow of a 2-dimensional unstable and laminar fluid through a branched artery with an aneurysm that was theoretically and computationally modelled utilising 3-dimensional geometry. Blood, a fluid with a high shear rate that is Newtonian, was employed in this simulation.

Philip et al. [18] Planning for surgical operations and evaluating potential treatment methods is made easier by analysis and prediction of the rupture risk of abdominal aortic aneurysms (AAA). Six idealised fusiform aneurysm models were examined at three distinct development phases, with a D_{max} of 3.5 cm, 4.25 cm, and 5 cm. These models ranged from high (shorter) to low (longer) values of the shape index.

Computational predictions of hemodynamic changes were performed considering idealised models for four severe proximal neck angulations of symmetric aneurysms, assuming conditions of laminar flow and a rigid artery wall [19]. The case of a 62-year-old lady who was transferred to our hospital due to stomach discomfort and had a history of kidney transplant 14 years before was given by Thanh et al. [20]. A 6 cm maximum diameter infrarenal fusiform abdominal aortic aneurysm and a 4 cm fusiform aneurysm in the left common iliac artery were both verified by computed tomography.

Wang et al. [21] evaluated the viability of machine learning-based pulse wave analysis for the early identification of AAAs. One-dimensional blood flow modelling was used to replicate pulse waves in the main systemic arteries. Kadhim et al. [22] developed a three-dimensional computational fluid dynamic model to investigate blood hydrodynamics and shear stresses at different cardiac cycles. A user-defined function (UDF) code was developed to model the valve leaflet motion.

This UDF updates the tetrahedral mesh according to the location of the valve leaflet, which enables the modelling of complicated moving geometries and achieves solution convergence with ease without the need to adjust the relaxation factor values. Valve leaflets and valve pivots were found to be continuously

exposed to shear stresses higher than 52.3 Pa, which, according to previous research findings, may cause damage to blood platelets.

The problem of the present study is the abdominal aortic aneurysm (FAAA) a vascular disease that happens due to the weakness of the aorta and its development in the artery wall like a balloon structure. Such developed a ballon-like effect on the blood flow hemodynamic characteristics, leading to serious health problems. Hence, the objective of this study is to predict the influence of the presence of fusiform abdominal aortic aneurysms FAAA with various geometries and configurations on the hemodynamic blood flow.

The investigations were performed experimentally and numerically to visualise the blood flow structure and to capture the friction factors and wall shear stress in the FAAA. The study considered varying the two axes of the FAAA of a semi-major axis, a, and a semi-minor axis, b of FAAA. Thus, the ratio of the FAAA to artery diameter ranged by D/d = 1.5, 2, 2.5, and 3.

In the computational simulation, 2D of sixteen models with saccular FFAAA and one without an aneurysm model saccular that must be an axisymmetric and stiff wall with Newtonian blood flow model were simulated numerically. The hemodynamic of the blood is deliberated as the steady state for a range of laminar Reynolds numbers of 260, 390, and 530. Blood hemodynamic is a calculated set of parameters consisting of the pressure drop Δp , wall shear stress, τ , dimensionless flow velocity, u/u_0 , and friction factor.

2. Problem Formulation

2.1. Experimental setup and methods

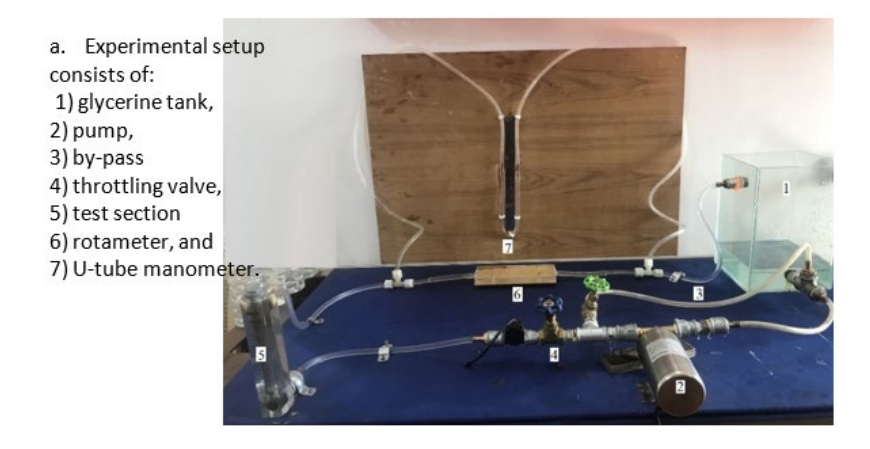
The present experimental approaches, as presented in Figs. 1(a) and (b), include a system of flow units to supply constant rates of the volume blood flow for the aortic aneurysm of humans and experiments are performed at 28 °C. The blood movement is directed with plastic hoses to the experimental test section that has fusiform abdominal aortic aneurysms replaced models with different geometries that are rigid, smooth, and symmetrically in shape.

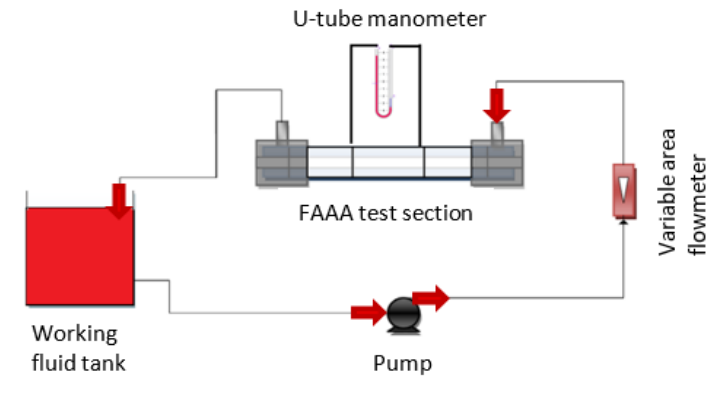
In this study the semi-major axis, that represents the longest radius of FAAA with dimensions of 18, 36, 54 and 72 mm, and semi-minor axis, b that represent the shortest radius of FAAA with dimensions of 7, 9, 12 and 14 mm. Thus, the ratio of the FAAA to artery diameter ranged by D/d = 1.5, 2, 2.5, and 3.

The test section is made from a transparent acrylic plastic block with a thickness of 10 mm, and the radius of the artery is R=5 mm. The length of the test section is selected as L=100 mm to achieve a fully developed flow and avoid the exit reflectance where the researcher assumes the dimensions used in the research.

In the blood flow downstream acclimatising of the test section, the blood flow enters the aneurysm models at a constant flow rate with three different values of 0.5, 1.5, and 2 LPM, corresponding to Reynold number values of 260, 390, and 530 according to the hemodynamic specification of blood flow in this artery of laminar flow. The pump used in this experimental work is a SAMGER water pump 110 V, 90 W water pressure booster pump, and water flow booster Armstrong pump for household shower with flow switch (60 HZ 15PSI).

The pressure drop is restrained by a U-tube manometer attendant in the downstream and upstream of the test section of the FAAA with 350 mm from the inlet and the outlet, respectively of the test section, which has an accuracy of 0.8 %. The flow rate is measured by a rotameter with a range of 1 - 7 LPM with uncertainty of ± 0.1 LPM. The working fluid is glycerine which has a physical property presented in Table 1.





b. Schematic diagram of the experimental testing setup

Fig. 1. The experimental setup.

2.2. Computational methodology

2.2.1. Computational model generation

The problem is solved considering 2-dimensional cylindrical flow, in r and x, incompressible, steady-state flow. It should be noted that ANSYS converts the cylindrical flow into cartesian, and the r and x-axis become y and x-axis. The boundary conditions are identified as shown in Fig. 2.

- At the inlet of the abdominal aorta along the r-axis, there is no radial flow, and pressure inlet boundary conditions are suitable for the present case, i.e., 2D simulation.
- No slip conditions at the wall. I.e., the velocity on the artery wall is zero.

Journal of Engineering Science and Technology December 2024, Vol. 19(6)

- At the inlet section of the domain, the pressure is fixed at 120 mm Hg, but along the exit section, it will be supposed that the 0 Pa is the value of the pressure outlet fixed as studied in the experimental part.
- Due to Fusiform, half of the computational domain is considered, where the boundary condition of the axisymmetric wall is imposed in the bottom boundary.

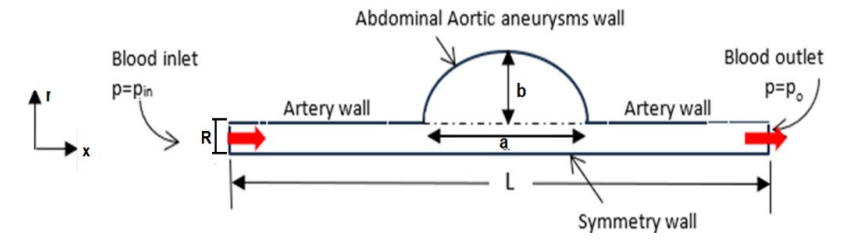


Fig. 2. The geometry and boundary conditions of the computational model.

For the ellipse having the transverse axis as the x-axis and the conjugate axis as the y-axis as presented in Table 1. The axis of the present shape is given by:

$$x^2a^2 + y^2b^2 = 1 (1)$$

Model	Dimensions		Model	Dimensions	
	a	b	Model	a	b
Smooth	0	0	Model-9	18	
Model-1	18	7	Model-10	36	12
Model-2	36		Model-11	54	12
Model-3	54		Model-12	72	
Model-4	72		Model-13	18	
Model-5	18	9	Model-14	36	1.4
Model-6	36		Model-15	54	14
Model-7	54		Model-16	72	
Model-8	72.				

Table 1. Dimensions of the models studied of the FAAA.

2.2.2. Meshing and independence check

The artery geometry was created by SOLIDWORKS 2018 for this project, and it was utilised to create mesh generation to investigate issues, as shown in Fig. 3. The blood's viscosity is constant at 3.5 cP. To solve the pair of pressure and velocity by utilising the finite volume approach, the governing Navier-Stokes equations using the SIMPLE algorithm in FLUENT, as recommended by Hussain et al. [17]. The convergence criterion for continuity and momentum components velocities, u and v, were set 10⁻⁵.

A grid dependency analysis was used to determine the final grid since it is well-known that the size and number of cells have an impact on how accurate the solution is. Results of the 250 Reynolds number bifurcation velocity distribution for four distinct grids were compared. The following grid number sizes were chosen as the solution without FAAA: the nodes are 523554, and using quad and pave grid type, the maximum number of iterations is 490.

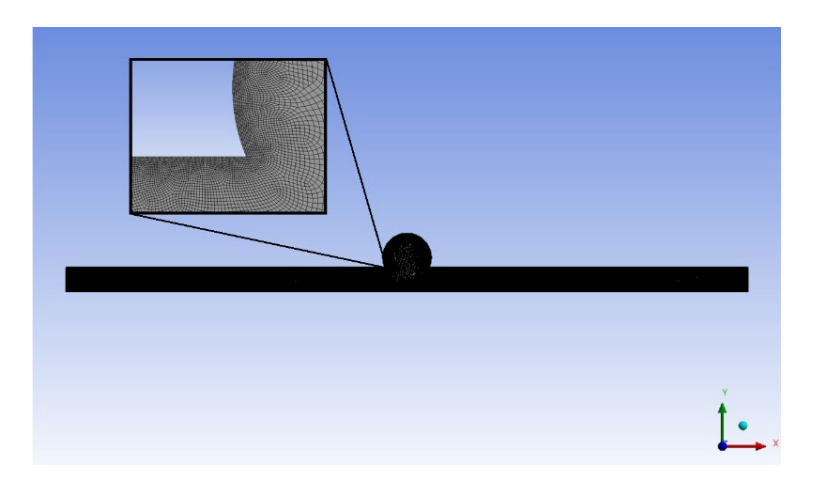


Fig. 3. Grid generated used in the present computational domain analysis.

Increasing the resolution and running the simulation again is the standard procedure for testing for grid independence. The original grid is probably fine if the findings do not drastically alter. If, however, there are significant differences between the two responses, the first grid was probably not resolved enough. Computations have been carried out for four selected grid sizes (i.e., 235654, 345216, 523554, and 856253), the summary of the grid independence test findings is presented in Table 2.

It was observed that the 523554 and 856253 nodes produced almost identical results with a percentage error of 0.08%. There is a significant disparity in the results, and as the number of elements increases, the friction values results begin to converge. After meshing structures d and e, the difference in the result value is very small. The (e) mesh has been chosen.

Mesh code	Number of nodes	Friction Factor	% of difference		
a.	235654	0.321			
b.	345216	0.311	3.2		
c.	523554	0.306	1.6		
d.	856253	0.304	0.65		
e.	942635	0.3039	0.001		

Table 2. Mesh dependency results in accuracy.

2.2.3. Governing equations

This work uses AAAs of the Fusiform type, in which the dilatation is symmetrical. Consequently, the numerical domain must be symmetrical. In this work, the computational domain is represented by a half-section of the artery and the FAAA. In contrast, the simulation domain has an artery with a central expansion that symbolises the FAAA.

In capillaries or small arteries, the non-Newtonian effects will appear in blood flow only (Fung [23]). In a recent simulation performed by Huang et al. [24], the blood flow problem is supposed to be homogeneous, incompressible, Newtonian, laminar flow, two-dimensional, steady, and fully developed. Blood is simulated as

glycerine fluid. Under these assumptions, the ANSYS-Fluent 19.0 solved the governing equations numerically, cylindrical coordinates system. However, following ANSYS axis notations, the governing equations are [25].

continuity equation:

$$\frac{\partial}{\partial x}(\rho u) + \frac{\partial}{\partial y}(\rho v) = 0 \tag{1}$$

Conservation of Momentum

x- direction (u- momentum)

$$\frac{\partial uu}{\partial x} + \frac{\partial vu}{\partial y} = -\frac{1}{\rho} \frac{\partial p}{\partial x} + \frac{1}{\rho} \frac{\partial}{\partial x} \left[\mu_{eff} \frac{\partial u}{\partial x} \right] + \frac{1}{\rho} \frac{\partial}{\partial y} \left[\mu_{eff} \frac{\partial u}{\partial y} \right] + S_u$$
 (2)

y- direction (v-momentum)

$$\frac{\partial vu}{\partial x} + \frac{\partial vv}{\partial y} = -\frac{1}{\rho} \frac{\partial p}{\partial y} + \frac{1}{\rho} \frac{\partial}{\partial x} \left[\mu_{eff} \frac{\partial v}{\partial x} \right] + \frac{1}{\rho} \frac{\partial}{\partial y} \left[\mu_{eff} \frac{\partial v}{\partial y} \right] - \frac{2}{3} \frac{\partial k}{\partial y} + S_v$$
 (3)

For a Newtonian model of blood hemodynamic, η is constant. The total pressure drop can be formed by the quantity of the pressure drop terms due to the viscous friction and due to the presence of the AAA effects as:

$$\Delta P = \frac{128}{\pi} \frac{\mu q}{D_h^4} L + \frac{kt}{2} \left[\left(\frac{A_2}{A_1} \right)^2 - 1 \right] \rho V |V| \tag{4}$$

Where L is the length of the artery model test section, consisting of the upstream, downstream, and test sections. Hence, L = 10D (upstream) + (test section) + 10D (downstream).

The friction factor of the blood flow is calculated from:

$$f = \frac{2D_h \,\Delta P}{L\rho u_0^2} \tag{5}$$

2.2.4. Simulation procedure

The finite volume method (FVM) was employed in this study to discretise the governing partial differential equations, yielding a set of linear algebraic equations. The field governing equations are solved using the commercial CFD solver ANSYS FLUENT version 19. A discretisation using the finite volume approach is based on an integral form of the partial differential equation to be solved (mass, momentum, or energy conservation rules). These equations are then discretised to generate a numerical analogue. After that, the domain is separated into little grids or elements.

The pressure values are obtained using the PRESTO (pressure staggering option) system, and the interaction between pressure and velocity is coupled using SIMPLE (Semi Implicit Method for Pressure Linked Equations). Lastly, the initial and boundary conditions of the problem are employed to solve these equations. The method of solution can be direct or iterative. Furthermore, some control parameters are employed to control the method's convergence, stability, and accuracy.

For the momentum and energy variables, a second-order upwind technique was used, and SIMPLE was used to couple the interaction between pressure and velocity. The tolerance for continuity and velocity was set to 1×10^{-6} , while the tolerance for energy was set to 1×10^{-8} .

3. Results and Discussion

3.1. Experimental results

Some observations and comments from the findings of a wider range of tested flow conditions and computed numerical simulation are made in the text that follows. It is logical to extrapolate from information gathered from idealised models alone to feel the flow patterns and provide an indicator for the blood hemodynamic in the FAAA aneurysm model. The experimental results of the friction factor with the Re are shown in Figs. 4 and 5. This figure gives the variation of friction factor for the arterial segment length with different values of Re.

The increase in Re will lead to a decreased friction factor. Model-3 with an elliptical ratio of (a/b = 0.38) semi-realistic aneurysms FAAA gives the maximum friction factor f = 0.246 as compared with the smooth model with an increasing per cent of 12 % at Re = 260. Figure 5 shows that Model-6 showed the maximum values of the friction factor f = 0.282 as compared with the smooth model, with an increasing percentage of 26% at Re = 260. Also, at Re = 560, the maximum values of the friction factor f = 0.18 at model-4 as compared with without an aneurysm smooth model of f = 0.138.

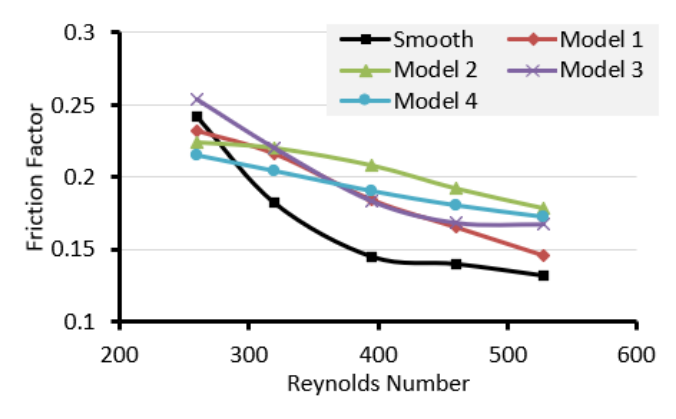


Fig. 4. Experimental friction factor for models with and without FAAA model-1 to model-4.

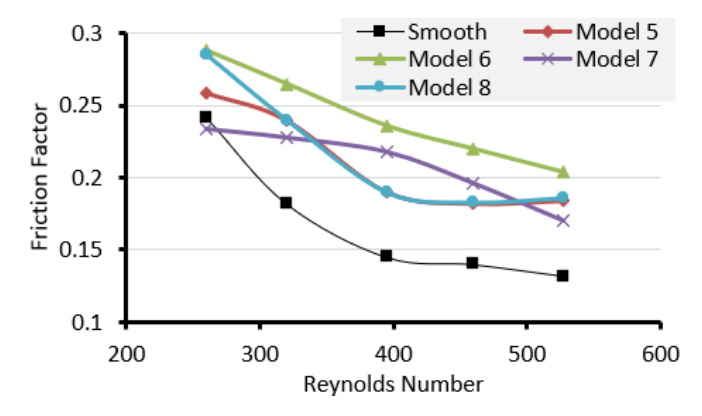


Fig. 5. Experimental friction factor for models with and without FAAA model-5 to model-8.

Journal of Engineering Science and Technology December 2024, Vol. 19(6)

3.2. Computational results

3.2.1. Validation of computational procedure

The computational procedure has been validated to build confidence in the developed computational procedure by comparison with physical measurements. The CFD results were compared with PIV data for a patient-specific aneurysm, aiming to comprehensively examine the flow agreement between the two approaches at a variety of flow rates and several locations in the aneurysm. The simulation prediction of blood flow behaviours obtained for the FAAA aneurysm model in simulations.

Table 3 shows the validation results between the numerical and experimental results of the recent study for smooth and Model-4 as a sample. The results show good agreement between the current numerical and the experimental results of [15], as the percentage of relative difference is 0.67% to 2.3% for smooth and from 0.54% to 2.5% for Model-4. These validation results confirm that the proposed assumptions were reasonable and close to reality.

Smooth Model-4 Model-4 Smooth Re Current By Reorowicz et al. Current By Reorowicz et al. **CFD CFD** 15] Experiment 15] Experiment 262 0.2164 0.22 0.2246 0.23 0.1533 0.16 0.219 0.23 394 525 0.1270 0.13 0.1755 0.18

Table 2. Validation by comparison with previous numerical and experimental results.

3.2.2. Velocity distribution results

The predicted axial velocity contours are plotted in Figs. 7 and 8 for all simulated cases listed in Table 2. Figure 6 presents the simulation results of all cases with FAAA height b equal to 14 mm. It plots the numerical results of velocity contours without the aneurysm model and models 1 to model-16. It showed the influence of FAAA on the contour of the velocity of the blood flows with the Newtonian model at Re = 390. Comparison between Figs. 6(a) and (b) demonstrates that the use of FAAA along the artery's upper wall will result in a novel flow pattern inside the FAAA zone.

The findings demonstrated that the recirculation vortex inside the FAAA got marginally stronger as the flow accelerated to the point of maximum flow rate close to the inner wall. This expanded the size of the recirculation zones and caused negative velocity gradients. However, it was demonstrated in the FAAA area of the aorta that the development of a minor motion of blood flow along the curvature of the vessel causes the introduction of the radial pressure gradient from the outer wall.

Effects of the model's type of FAAA on velocity contour can be shown clearly in Fig. 7. The increase in the vessel and reduced momentum and the blood pressure in the FAAA location will verify the upturned blood flow in the FAAA inner region. In the region immediately outside the FAAA, the blood velocity contours are no longer parallel. However, a region of flow separation immediately beyond the blood artery constriction is where the laminar flow is most disrupted. The

findings indicated that there is a flow stream separation zone inside the FAAA in the bulge where velocities are low, and flow reversal occurs.

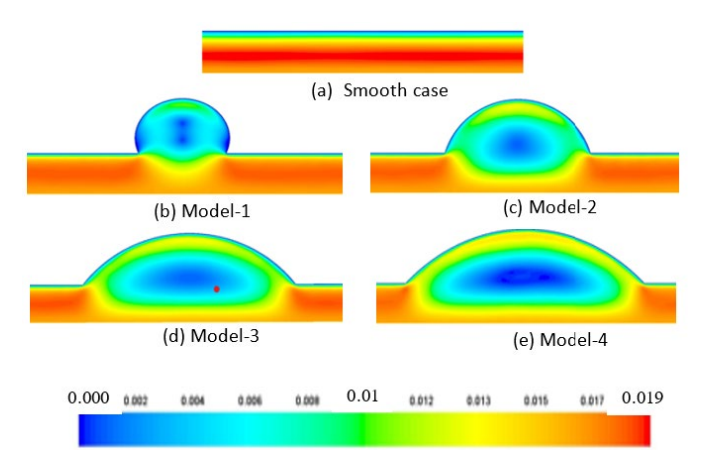


Fig. 6. Contour of velocity magnitude for smooth a and Models-1 to Model-4, with b = 14 mm, at Re = 390

Additionally, it was demonstrated that the separation of the fluid layer next to the wall caused by an increase in Reynolds number would enhance the reversed flow in the FAAA near the artery wall. Separating the flow between the exterior and interior FAAA arteries required raising the Reynolds number to 530. According to the findings, the flow was completely established in the area just before the abdominal aorta. However, the velocity was biased toward the heat of the FAAA in the FAAA. Along the FAAA wall, the low momentum area was discovered.

The blood flow was decelerated due to an increase in the artery's blood flow area in the FAAA region when flow entered the distal, and it was also evident that the flow reaccelerated correspondingly after entering the proximal.

As compared between Fig. 7(b) of model-1 and Fig. 7(e) of model-4, with increasing a semi-major axis, a that represents the longest radius of FAAA, it showed that the dynamic vorticity of the velocity will elongate with the size of the FAAA, and the velocity becomes lower in the middle of this vorticity.

The Reynolds number values in peripheral arteries are under the critical standard value. However, the circulatory system arteries are not smooth, ideal, or straight vessels but it was enlarged, bent, and with irregularities to their surface and abrupt diameter changes. These features can make the blood flow more disturbed and turbulent. The velocity profile becomes skewed at areas where the vessel curves or FAAA. It showed that the presence of the aneurysm in the blood flow bath across the abdominal aorta would case increase the velocity stream at the same flow condition as laminar flow.

The effect of increasing a semi-minor axis, b that represents the shortest radius of FAAA on the velocity contour is presented in Fig. 7 for the laminar flow Newtonian blood model at Re = 290. The results showed that the magnitude of velocity in the region of the FAAA at the inner wall zone is growing as the cross-section area increases, which would significantly increase the inner pressure acting on the inner FAAA wall and thus raise the likelihood of FAAA rupture.

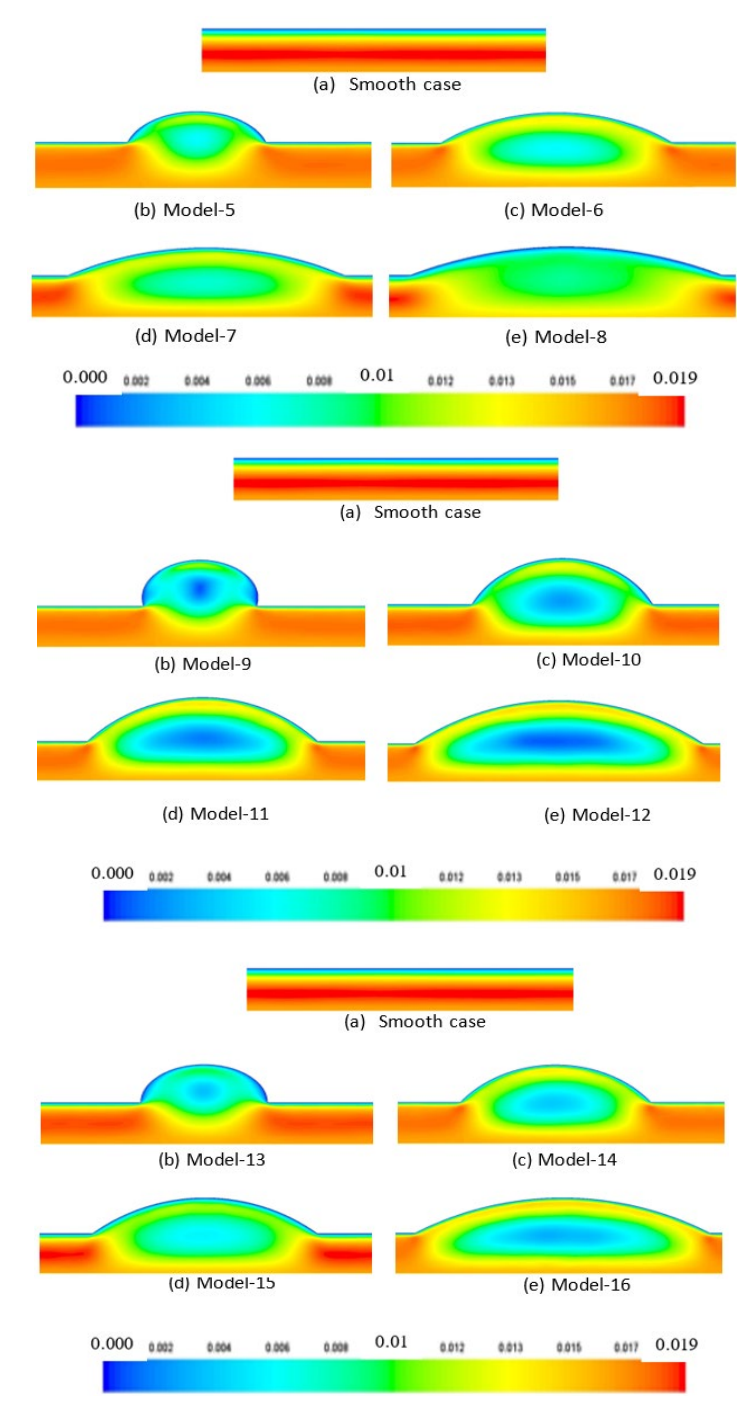


Fig. 7. Contours of velocity magnitude for smooth and Models-1 to Model-16, at Re = 290.

Figures 8(a) to (e) display the Newtonian blood flow simulation at the centre location inside the FAAA zone at x/L = 0.5. The effects of sixteen FAAA model

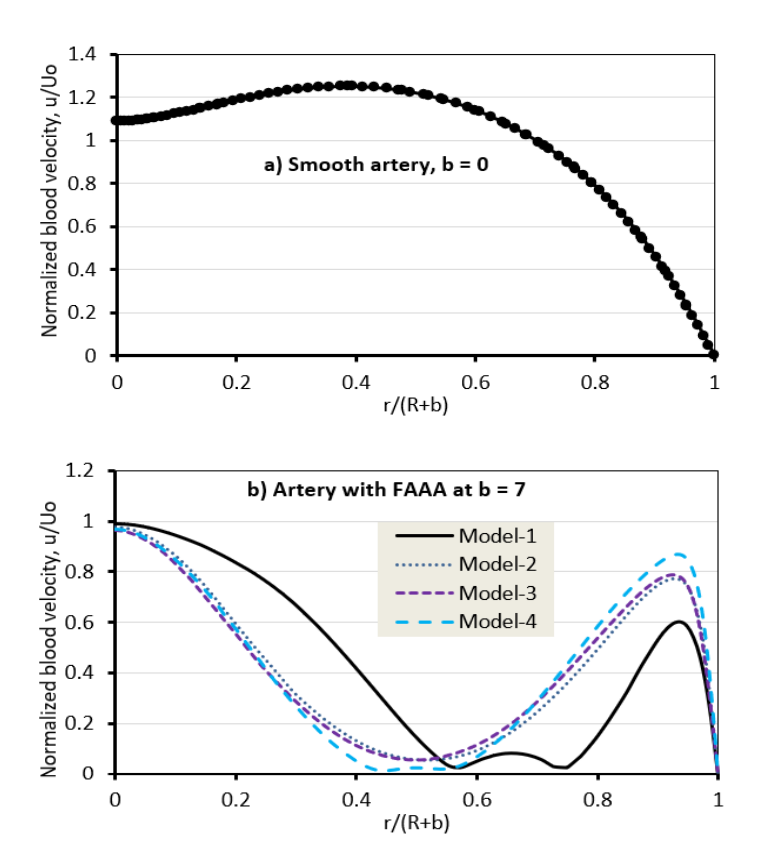
Journal of Engineering Science and Technology December 2024, Vol. 19(6)

simulations on dimensionless velocity (u/U_o) in the r-direction are studied. The blood velocity is normalised by dividing over the mean inlet velocity, U_o . However, the figures demonstrate that if the inner diameters of the artery vessels varied throughout the blood flow stream in the r-direction, the overall profile would alter from one point to the next. It has been demonstrated that at the location of the flow at the smooth model of b=0 and r/(R+b)=0.4, as shown in Fig. 8(a) without FAAA.

The results showed that the maximum normalised velocity decreased from u/U_o = 1.2 to 0.59, 0.75, 0.78, and 0.86 at r/(R+b) = 0.93 and b = 7, for with FAAA Model-1, Model-2, Model-3, and Model-4, respectively, as shown in Fig. 8(b) due to increasing the frontal area of the artery area and this will lead to decrease the velocity inside the FAAA.

The larger artery diameter in the FAAA area would result in a decrease in the maximum velocity of a laminar flow state and a flatter fluctuation profile. The dimensionally inert velocity profile at the arterial bifurcation's entry. Also, it shows that there are three sites for the zero's velocity rather than only two. In the case of laminar flow, there is no change in velocity profile between the two cases, but when increasing the blood Reynolds number to 530, the velocity decreased in the case without FAAA.

The FAAA causes the flattened velocity profiles but is less evident than the typical M-shape velocity profiles and after entering the FAAA, the velocity peak is moved towards the inner wall. However, in the case of FAAA the profile has more fluctuation in flow condition than that in the laminar flow condition.



Journal of Engineering Science and Technology December 2024, Vol. 19(6)

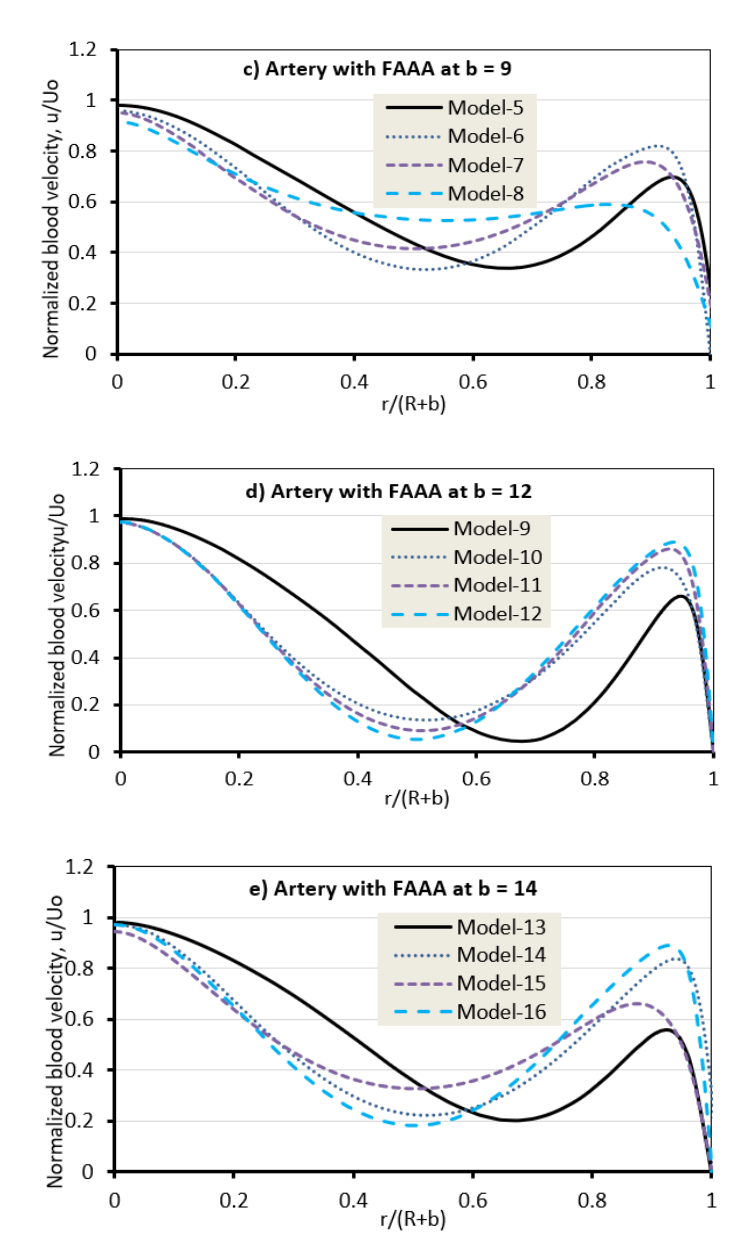


Fig. 8. Variation of normalised stream velocity (u/U_0) with radial artery distance without FAAA case, at Re = 360.

3.2.3. Friction factor

The friction factor was shown with the x-axis along the upper wall of the artery in two cases (with and without FAAA) using just four models to enhance the attention on the aneurysm areas. According to Figs. 9(a) and (b), the presence of the FAAA would increase the pressure drop on the top wall of the FAAA region, and the profiler of blood velocity was blunt when associated with the situation with and without the FAAA, which would subsequently increase the friction factor.

In general, the larger cross-sectional flow area and augmented FAAA radial detachment zone caused the static pressure to drop in the case of FAAA. The existence of FAAA makes the friction factor increase, and it has two highest points in the two areas of the FAAA's entrance and departure. As the radial distance of the artery aneurysm area increases, the friction factor gradually decreases near the FAAA inner wall.

It shows that the existence of an aneurysm causes the static pressure to rise along the FAAA's inner wall, which has a changing shape in the vicinity of the inner wall of the FAAA with low separation momentum. It demonstrated that, when compared to the other models, model-4 provides the highest friction factor by about 72 % as compared with the without an FAAA model and this is bad for the circulatory system due to increasing the FAAA artery fracture rate.

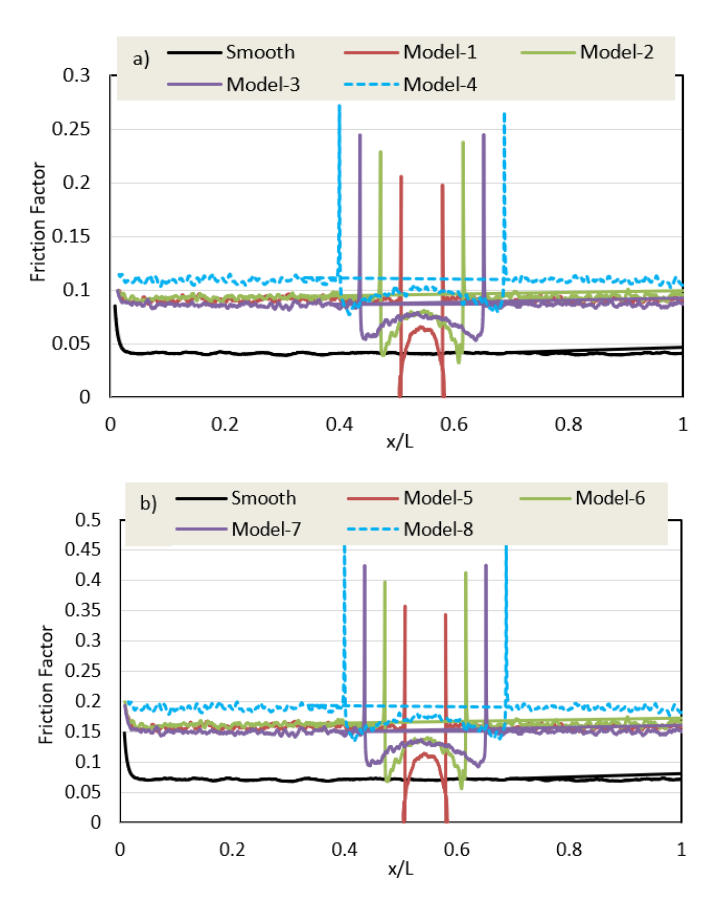


Fig. 9. Relation between friction factor with the axial artery length for various FAAA models.

4. Conclusions

Sixteen models of FAAA have been investigated experimentally and computationally to examine changes in the semi-major and semi-minor axes of Fusiform Abdominal Aortic Aneurysms (FAAA) as well as the shortest radius of FAAA. The study has been conducted at different Reynolds values for Newtonian

laminar blood flow. The findings show that the FAAA border geometry's wall configuration has an impact on the hemodynamic patterns.

The experimental findings indicate that as the semi-major axis decreases and the semi-minor axis grows, the friction factor rises. The numerical results show that the highest values of wall shear stress and friction factor were found upstream and downstream of FAAA. When FAAA is present in the flow path, the dimensionless velocity of distal decreases by 33% for Model-1 and by 51% for Model-4.

Also, test models with $a=36 \, \text{mm}$ and $b=7 \, \text{mm}$ yield the largest friction factor. Additionally, the data show that the highest variation speed and the formation of some vortices are situated near the FAAA's inner wall and offer some insightful information on the blood flow and shear stress within the structure. When compared to models without an FAAA, model-4 offers the largest friction factor by roughly 72% compared to bare, or smooth, case, which is detrimental to the circulatory system since it raises the risk of FAAA artery fractures.

```
Nomenclatures
              The length of the FAAA, mm
              The height of the FAAA, mm
b
D
              abdominal aorta inner diameter, mm
              fanning friction factor.
              gravitational acceleration, m/s<sup>2</sup>
g
L
              Total length of test section, mm
              pressure, Pa
p
R
              The artery radius, mm
              coordinate of the radial axis
U_o
              Mean axial velocity bulk inlet, m/s
              x-direction velocity component, m/s
и
              r-direction velocity component, m/s
ν
              axial distance of artery model, mm
х
Greek Symbols
              viscosity, Pa.s
λ
              constant of time, s
              rate of shear stress, s-1
γ
              blood viscosity
η
              gradient.
Δ
              density, kg/m<sup>3</sup>
ρ
              shear stress, N/m<sup>2</sup>)
              kinematic viscosity, m<sup>2</sup>/s
1)
              tensor of stress
Abbreviations
AAA
              Abdominal Aortic Aneurysms
FAAA
              Fusiform Abdominal Aortic Aneurysms
FEM
              Finite Element Method
PIV
              Particle Image Velocity
WSS
              Wall Shear Stress
```

References

- 1. Cowan, J.A.; Dimick, J.B.; Henke, P.K.; Rectenwald, J.; Stanley, J.C.; and Upchurch, G.R. (2006). Epidemiology of aortic aneurysm repair in the United States from 1993 to 2003. *Annals of the New York Academy of Science*, 1085(1), 1-10.
- 2. Yu, S.C.M. (2000). Steady and pulsatile flow studies in Abdominal Aortic Aneurysm models using particle image velocimetry. *International Journal of Heat and Fluid Flow*, 21(1), 74-83.
- 3. Fillinger, M.F.; Marra, S.P.; Raghavan, M.L.; and Kennedy, F.E. (2003). Prediction of rupture risk in abdominal aortic aneurysm during observation: Wall stress versus diameter. *Journal of Vascular Surgery*, 37(4), 724-732.
- 4. Peattie, R.A.; Riehle, T.J.; and Bluth, E.I. (2004). Pulsatile flow in fusiform models of abdoiminal aortic aneurysms: flow fields, velocity patterns and flow-induced wall stresses. *Journal of Biomechanical Engineering*, 126(4), 438-46.
- 5. Deplano, V.; Knapp; Y.; Bertrand, E.; and Gaillard, E. (2007). Flow behaviour in an asymmetric compliant experimental model for abdominal aortic aneurysm. *Journal of Biomechanics*, 40(11), 2406-2413.
- 6. Molla, M.M. (2009). LES of pulsatile flow in the models of arterial stenosis and aneurysm. PhD Thesis, Department of Mechanical Engineering, University of Glasgow.
- 7. Altuwaijri, O. (2012). Advanced computer modeling of abdominal aortic aneurysms to predict risk of rupture. PhD Thesis, Department of Engineering, The University of Hull.
- 8. Hemmler, A.; Lutz, B.; Reeps, C.; Kalender, G.; and Gee, M.W. (2018). A methodology for in silico endovascular repair of abdominal aortic Aneurysms. *Biomechanics and Modelling in Mechanobiology*, 17(4), 1139-1164.
- 9. Jayendiran, R.; Condemi, F.; Campisi, S.; Viallon, M.; Croisille, P.; and Avril, S. (2020). Computational prediction of hemodynamical and biomechanical alterations induced by aneurysm dilatation in patient-specific ascending thoracic aortas. *International Journal of Numerical Methods Biomedical Engineering*, 36(6), e3326.
- 10. Bauer, A.; Bopp, M.; Jakirlic, S.; Tropea, C.; Krafft, A.J.; Shokina, N.; and Hennig, J. (2020). Analysis of the wall shear stress in a generic aneurysm under pulsating and transitional flow conditions. *Experiments in Fluids*, 61(2), 59.
- 11. Afrouzi, H.H.; Ahmadian, M.; Hosseini, M.; Arasteh, H.; Toghraie, D.; and Rostami, S. (2020). Simulation of blood flow in arteries with aneurysm: Lattice Boltzmann Approach (LBM). *Computer Methods and Programs in Biomedicine*, 187, 105312.
- Dubey, A.; Vasu, B.; Anwar Bég, O.; Gorla, R.S.R.; and Kadir, A. (2020). Computational fluid dynamic simulation of two-fluid non-Newtonian nanohemodynamics through a diseased artery with a stenosis and aneurysm. Computer Methods in Biomechanics and Biomedical Engineering, 23(8). 345-371.
- 13. Wang, H.; Krüger, T.; and Varnik, F. (2019). Effects of size and elasticity on the relation between flow velocity and wall shear stress in side-wall aneurysms: A lattice Boltzmann-based computer simulation study. *PLoS ONE*, 15(1), e0227770.

- 14. Djorovic, S.; Koncar, I.; Davidovic, L.; Starcevic, S.; and Filipovic, N. (2018). Computational analysis of blood flow characteristics in an aortic system with abdominal and left common iliac aneurysm pre- and post-stent grafting. *EAI Endorsed Transactions on Pervasive Health and Technology*, 4(13), e4.
- 15. Reorowicz, P.; Tyfa, Z.; Obidowski, D.; Wiśniewski, K.; Stefańczyk, L.; Jóźwik, K.; and Levy, M.L. (2022). Blood flow through the fusiform aneurysm treated with the flow diverter stent-Numerical investigations. *Biocybernetics and Biomedical Engineering*, 42(1), 375-390.
- Panchal P.M.; Hathi, D.S.; Shah, N.K.; and Lakdawala, A.M. (2022). A numerical study on pulsatile non-Newtonian hemodynamics in doublefusiform abdominal aortic aneurysms. *Physics of Fluids*, 34(3), 031908.
- 17. Hussain, A.; Naveel Riaz Dar, M.; and Tag-eldin, E.M. (2023). Mathematical analysis of unsteady blood flow through bifurcated abdominal aorta featured aneurysm. *Alexandria Engineering Journal*, 75, 589-604.
- 18. Philip, N.T.; Patnaik, B.S.V.; and Sudhir, B.J. (2022). Hemodynamic simulation of abdominal aortic aneurysm on idealised models: Investigation of stress parameters during disease progression. *Computer Methods and Programs in Biomedicine*, 213, 106508.
- Kaewchoothong, N.; Algabri, Y.A.; Assawalertsakul, T.; Nuntadusit, C.; and Chatpun, S. (2022). Computational study of abdominal aortic aneurysms with severely angulated neck based on transient hemodynamics using an idealised model. *Applied Science*, 12(4), 2113.
- 20. Thanh, V.T.; Bang, H.T.; Phat, N.D.; Cuong, L.T.; Dinh, L.Q.; Thuy, T.T.M.; and Vy, T.T. (2020). Endovascular repair for abdominal aortic aneurysm in a kidney transplant recipient. *Radiology Case Reports*, 15(12), 2655-2659.
- 21. Wang, T.; Jin, W.; Liang, F.; and Alastruey, J. (2021). Machine learning-based pulse wave analysis for early detection of abdominal aortic aneurysms using in silico pulse waves. *Symmetry*, 13(5), 804.
- 22. Kadhim, S.K.; Nasif, M.S.; Al-Kayiem, H.H.; and Al-Waked, R. (2018). Computational fluid dynamics simulation of blood flow profile and shear stresses in bileaflet mechanical heart valve by using monolithic approach. *Simulation*, 94(2), 93-104.
- 23. Fung, Y.-C. (1993). *Biomechanics: Mechanical properties of living tissues*. Springer New York, NY.
- 24. Huang, J.; Holt, R.G.; Cleveland, R.O.; and Roy, R.A. (2004). Experimental validation of a tractable numerical model for focused ultrasound heating in flow-through tissue phantoms. *The Journal of the Acoustical Society of America*, 116(4), 2451-2458.
- 25. Fluent release 6.2.16, Fluent Incorporated, 2005.